Geoscience Frontiers 10 (2019) 1029–1037

HOSTED BY

Contents lists available at ScienceDirect

China University of Geosciences (Beijing)

Geoscience Frontiers

journal homepage: www.elsevier.com/locate/gsf

Research Paper

# Timings of early crustal activity in southern highlands of Mars: Periods of crustal stretching and shortening

Trishit Ruj [a,b,*], Goro Komatsu [a], Jan Hendrik Pasckert [c], James M. Dohm [d]

[a] International Research School of Planetary Sciences, Università d'Annunzio, Viale Pindaro 42, 65127, Pescara, Italy
[b] Department of Earth and Planetary Science, School of Science, University of Tokyo, Hongo 7-3-1, Bunkyo, Tokyo 113-0033, Japan
[c] Institut für Planetologie, Westfälische Wilhelms-Universität, Wilhelm-Klemm-Str. 10, 48149, Münster, Germany
[d] Foundation for Advancement of International Science, 24-16, Kasuga, 3-chome, Tsukuba, Ibaraki, 305-0821, Japan

ARTICLE INFO

*Article history:*
Received 7 November 2017
Received in revised form
6 April 2018
Accepted 27 May 2018
Available online 28 June 2018
Handling Editor: Stijn Glorie

*Keywords:*
Martian dynamics
Southern highlands
Extensional tectonics
Compressional tectonics
Age of structures
Buffer crater counting

ABSTRACT

Extensional and compressional structures are globally abundant on Mars. Distribution of these structures and their ages constrain the crustal stress state and tectonic evolution of the planet. Here in this paper, we report on our investigation over the distribution of the tectonic structures and timings of the associated stress fields from the Noachis-Sabaea region. Thereafter, we hypothesize possible origins in relation to the internal/external processes through detailed morphostructural mapping. In doing so, we have extracted the absolute model ages of these linear tectonic structures using crater size-frequency distribution measurements, buffered crater counting in particular. The estimated ages indicate that the tectonic structures are younger than the mega impacts events (especially Hellas) and instead they reveal two dominant phases of interior dynamics prevailing on the southern highlands, firstly the extensional phase terminating around 3.8 Ga forming grabens and then compressional phase around 3.5–3.6 Ga producing wrinkle ridges and lobate scarps. These derived absolute model ages of the grabens exhibit the age ca. 100 Ma younger than the previously documented end of the global extensional phase. The following compressional activity corresponds to the peak of global contraction period in Early Hesperian. Therefore, we conclude that the planet wide heat loss mechanism, involving crustal stretching coupled with gravitationally driven relaxation (i.e., lithospheric mobility) resulted in the extensional structures around Late Noachian (around 3.8 Ga). Lately cooling related global contraction generated compressional stress ensuing shortening of the upper crust of the southern highlands at the Early Hesperian period (around 3.5–3.6 Ga).



## 1. Introduction

Crustal accumulation of Mars initiated immediately after its origin at around 4.6 Ga (Baker et al., 2007) accompanied by planet wide heat loss processes including lithospheric extension, volcanism and impact-related stresses. Extensional stresses resulted in the formation of the grabens (opposite facing parallel normal faults), normal faults. Cooling of the planet interior created a net global contraction resulting compressional stresses that lead to the formation of wrinkle ridges, lobate scarps (Mangold et al., 2000; Anderson et al., 2001). Occasionally, such structures are also hypothesized to be invoked by the 'tectonics and loading model' related to large-scale, tectono-magmatic complexes such as in Tharsis and related components (Carr, 1973; Watters, 1993; Mège and Masson, 1996; Nahm and Schultz, 2011). The southern highlands being one of the oldest crustal regions of Mars are expected to preserve history of early crustal state stress and interior dynamics, including volumetric adjustments related to long term cooling for a greater span of time (Baker et al., 2002, 2007).

Grabens, wrinkle ridges and lobate scarps are the most dense (hence dominated) and well-established stress indicators in the mapping area (Supplementary file 1). Grabens from two different areas (in the Terra region), wrinkle ridges from four different locations and lobate scarps from two other locations were selected for estimating ages using the Crater Size Frequency Distribution (CSFD), Buffered Crater Counting (BCC) technique to be precised (Supplementary file 2). Although the grabens in the two areas have different orientations (their general trends at an angle of 120° to

* Corresponding author. Department of Earth and Planetary Science, School of Science, University of Tokyo, Hongo 7-3-1, Bunkyo, Tokyo 113-0033, Japan.
*E-mail address:* trishit@irsps.unich.it (T. Ruj).
Peer-review under responsibility of China University of Geosciences (Beijing).

https://doi.org/10.1016/j.gsf.2018.05.016

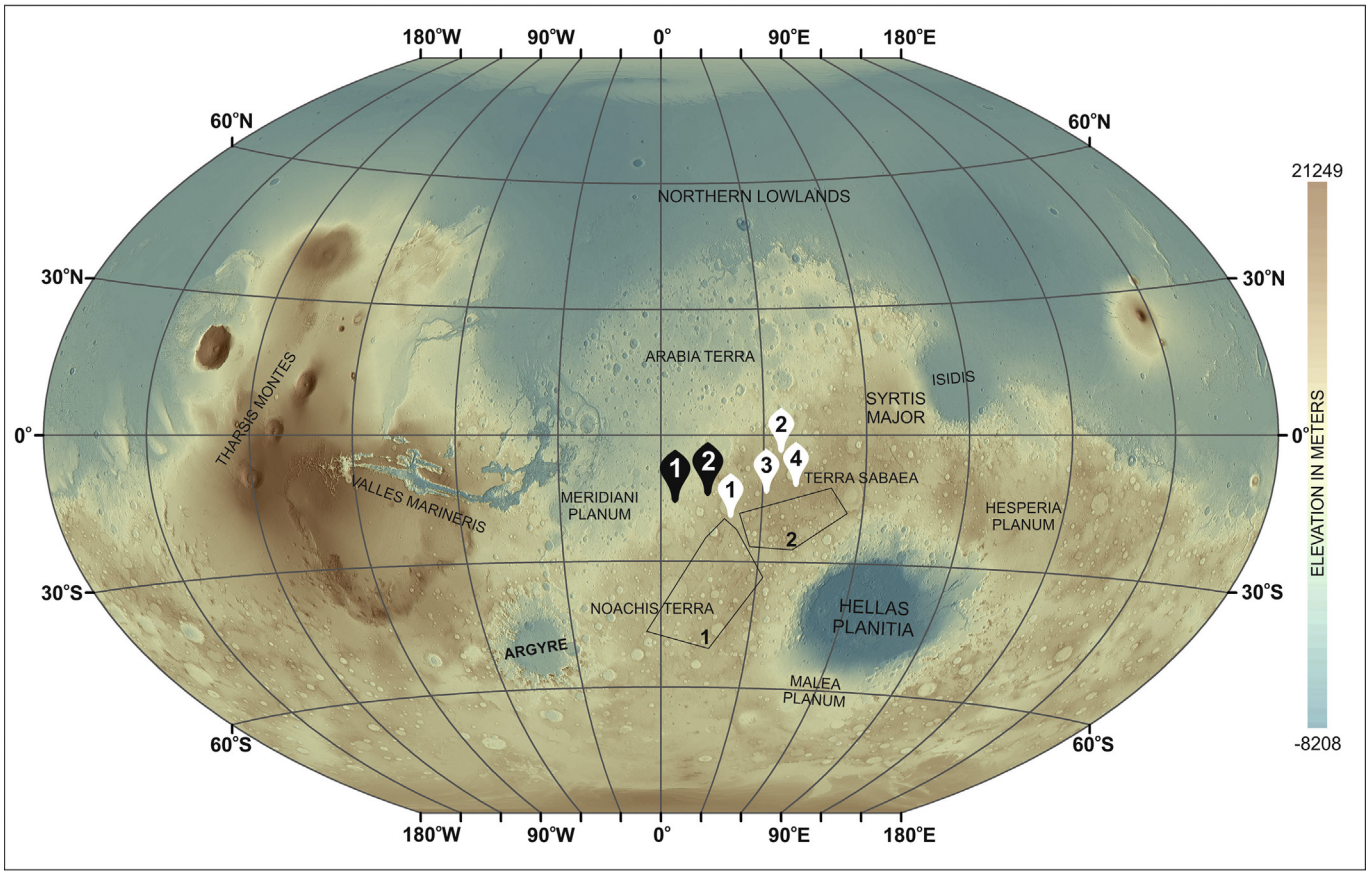


**Figure 1.** Global (MOLA hillshade overlaid on MOLA DEM) map showing the areas of interest. Quadrilateral shaped boxes indicate studied graben areas. Tear drop shaped markers indicate locations of the dated wrinkle ridges (white drops and black numbers) and lobate scarp (black drops and white numbers).

each other, Ruj et al., 2017), their BCC derived absolute model ages (AMAs) (Ivanov et al., 2001; Michael and Neukum, 2010) are very similar (around 3.8 Ga). Similar BBC derived ages and multiple orientations of the grabens indicate internal-driven activity into the Late Noachian epoch. These derived ages imply that termination of internal lithospheric activity is moderately younger (around 100 Ma) than the previously suggested end of dynamic activity (i.e., 3.93 Ga by Baker et al., 2007). Wrinkle ridges (Chicarro et al., 1985) and lobate scarps with similar trends over such a large part of the southern hemisphere signify presence of a regional compressional stress field was active over an extensive region in similar time i.e., 3.5–3.6 Ga. This later stress also corresponds to the large-scale cooling related global contraction as indicated by Mangold et al. (2000) and Andrews-Hanna et al. (2008). However, Nahm and Schultz (2011) strongly argued the origin of compressional stress is due to Tharsis induced tectonics.

Here in this paper, we report on the morphostructural map (Supplementary file 1) and the ages of dominant stress indicating structures from the southern highlands. However, these structural features are windows to the early Martian crustal evolution, driven by internal activity related to planetary heat loss mechanism and preferably influenced by a dynamic dynamo and associated magnetosphere (Baker et al., 2002, 2007; Connerney et al., 2005).

## 2. The area and geological background

### 2.1. Study area

Our study area (Supplementary file 1) covers a major part of the southern highlands, including the northern part of Noachis Terra, the central and southern parts of Terra Sabaea, parts of Tyrrhena Terra and the entire Hellas basin area (Fig. 1). Volcanic regions such as Syrtis Major Planum and Hesperia Planum, Malea Planum respectively occur to the north, to the east and to the south of the mapped region. The studied region is surrounded by mega impacts such as Argyre to the southwest, Isidis to the northeast. Arabia Terra and Meridiani Planum border northern and western side of the investigated region.

Based on CSFD measurements, the Hellas impact is estimated to have occurred around 3.99 ± 0.01 Ga (Werner, 2008), Isidis is of a similar age at 3.96 ± 0.01 Ga (Werner, 2008). Argyre impact has been estimated to be 3.93 Ga (Robbins et al., 2013) or 3.83 ± 0.01 Ga by Werner (2008). The new global geological map (Tanaka et al., 2014) indicates that the study region is covered by Early to Late Noachian highland rock materials, with some local occurrences of Amazonian/Hesperian impact craters and associated thick ejecta deposits. The ancient Noachian continental crust is partly covered by ejecta deposits from the giant impacts such as Hellas (Smith et al., 1999; Zuber et al., 2000), which have been differentially eroded through time exposing the more ancient continental crust in places.

### 2.2. Structures and their characterization and distribution

We mapped (Supplementary files 1 and 2) the distinct surface features and categorized them on the basis of morphologic dissimilarities and orientations (Ruj et al., 2017). The map (Supplementary file 1) shows the distribution of grabens to the west and north of the Hellas basin. Grabens of area 1 (grabens of Noachis Terra) and area 2 (grabens of Terra Sabaea) were grouped

separately due to their distinct morphologic pattern and orientation trend (antithetic to the Hellas basin outer rim curvature) (details of graben classification in Ruj et al., 2017 and Supplement file 2). NNE–SSW trending area 1 grabens have a maximum length and width of 1200 km and 100 km respectively. ENE–WSW trending area 2 grabens are individually smaller in length with respect to area 1 grabens but still form a trail of grabens that extends nearly 1500 km. Individual graben lengths are 250–300 km, with a nearly constant width of around 30 km. Olivine (Ody et al., 2013; Rogers and Nazarian, 2013) and pyroxene (Rogers and Nazarian, 2013) were reported from the both graben (Fig. 2a) floors. Ody et al. (2013) also believed that these graben floors are of Hesperian aged, however, Rogers and Nazarian (2013) argued that the basaltic material in the graben floor are products of Noachian volcanism. Since, our main concern was to extract the age of the grabens, we analyzed craters that are only in relation (both crosscutting and overprinting ejecta) with the graben bounding normal faults (discussed in details in Supplementary file 2). Both area 1 and 2 grabens trend antithetic to the Hellas basin's outer arc curvature.

Wrinkle ridges (Fig. 2b) occur on the volcanic plains of the northern and northwestern parts of the mapped region (Chicarro et al., 1985; Mangold et al., 2000), with a relatively consistent NNW–SSE orientation. Wrinkle ridges around Syrtis Major and Hesperia Planum were kept out of consideration of age determination due to their origins related to the gravitational collapse associated to the basin relaxation and sedimentation (Hiesinger and Head, 2004). Wrinkle ridges dominate mostly the northern and central part of Terra Sabaea (Ruj et al., 2017); while in the rugged central and southern part of the mapped region (i.e., Noachis Terra) lobate scarps are observed (Fig. 2c). However, both the wrinkle ridges and the lobate scarps follow the similar NNW–SSE trend. The contrasting style of the deformation between smooth plain volcanic sequences and highland materials reflects different responses to the mechanical and rheological property of the underneath material in both the presence (wrinkle ridges) and absence of layering (lobate scarp) (Watters, 1993; Mueller and Golombek, 2004). Therefore, layering in the frictionless scenario starts to fold in response to contraction, whereas, massive highlands in absence of layers develop lobate scarps (Ruj et al., 2018). The behavior of compressional force leads to thin or thick-skinned tectonics (combination of faulting and folding) (Plescia and Golombek, 1986; Mangold et al., 1998) in a different basement rock rheology in the presence or absence of volcanic materials (Watters, 1993).

### 2.3. Background evolution history

Tectonic evolution models of Mars mainly accounts for two major crustal elements: Tharsis and its components and the dichotomy boundary that separates the northern lowlands from the southern highlands. Ages determined by impact crater density indicate that both of these elements came into existence in the early history of Martian evolution, possibly due to an early dynamo/magnetosphere (Sleep, 1994) and a global hydrological cycle including an ocean as well as plate tectonism (Baker et al., 2007). This hypothesis includes the interaction among continental crustal materials, atmosphere and the ocean, conditions conducive to life on Earth referred to as the 'Habitable Trinity' (Dohm and Maruyama, 2014). The tectonic activity decreased over time and was concentrated at distinct localities at different times (Anderson et al., 2001, 2008). However, Baker et al. (2007) and Dohm (2017) proposed six major stages of crustal evolution with plate tectonics having played a significant role in the evolution of the planet in accordance with the ABEL (advent of bio-elements; using the mineral chemistry, U–Pb geochronology from Apollo 14 melt breccia zircons; Hopkins and Mojzsis, 2015) model proposed by Maruyama and Ebisuzaki (2017). This ABEL model proposes that the terrestrial planets (after the birth of the planet with extensive bombardment around 4.56–4.53 Ga and Mars started to solidified after possible presence of magma ocean) initiated (due to extensive bombardment resulted early tectonic activity by destroying stagnant lid condition) a proto-plate tectonic activity around 4.37 to 4.2 Ga forming an ocean-atmosphere system. Subsequently, accretion (subduction and the suturing of oceanic basins) played a significant role in the thickening of the continental crust, which includes the present-day southern-cratered highlands interpreted to be a remnant early supercontinent (tonalite-trondhjemite-granodiorite rich crust). Sleep (1994) also proposed that the southern highlands and the northern lowlands are products of the early Martian plate tectonics. The proposed evolution model by Baker et al. (2007) infers that the dynamo terminated prior to the Hellas impact with subsequent cessation of plate tectonic activity around the Argyre impact event followed by tectonism mainly related to episodic, stagnant-lid 'super-plume' phases especially associated with the evolution of Tharsis. This theory differs from the endogenic hypothesis by Sleep (1994), with the 'five stages of tectonic structures' reported by Golombek and Phillips (2010) and Argyre-impact-driven plate tectonism (Yin, 2012).

Non-primitive compressive stresses came into existence after the crust was formed and initial extensional tectonics for some

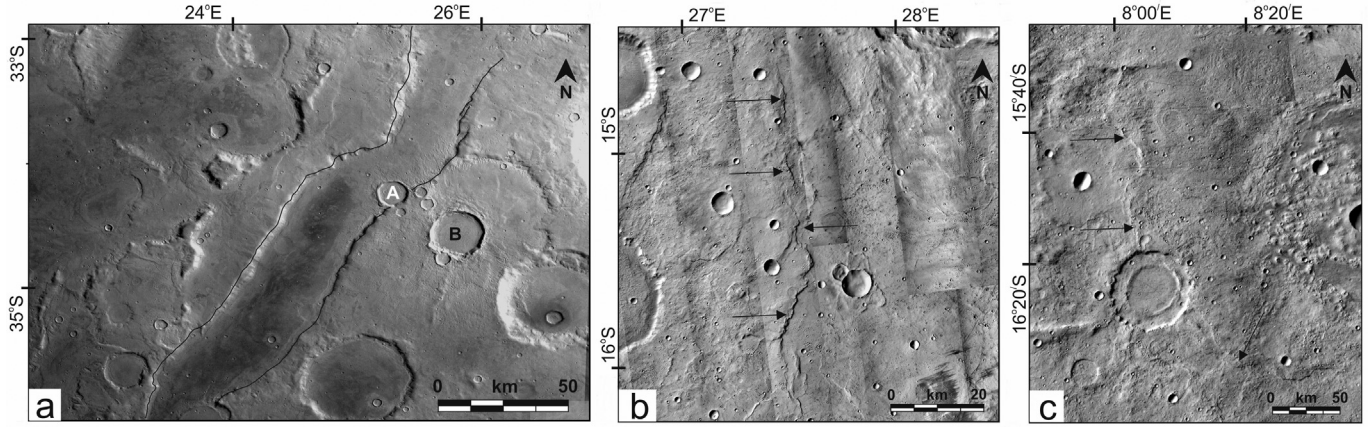


**Figure 2.** Extensional and compressional structures in Hellas Planitia and surrounding regions. (a) Graben of area 1. Crater A is observed to be overlapped over the graben wall, while Crater B is not overlapped but it's ejecta is on the graben floor. Therefore, both of these craters were taken into consideration. (b) Wrinkle ridge is marked with arrowheads. (c) Lobate scarp in the Terra Sabaea region.

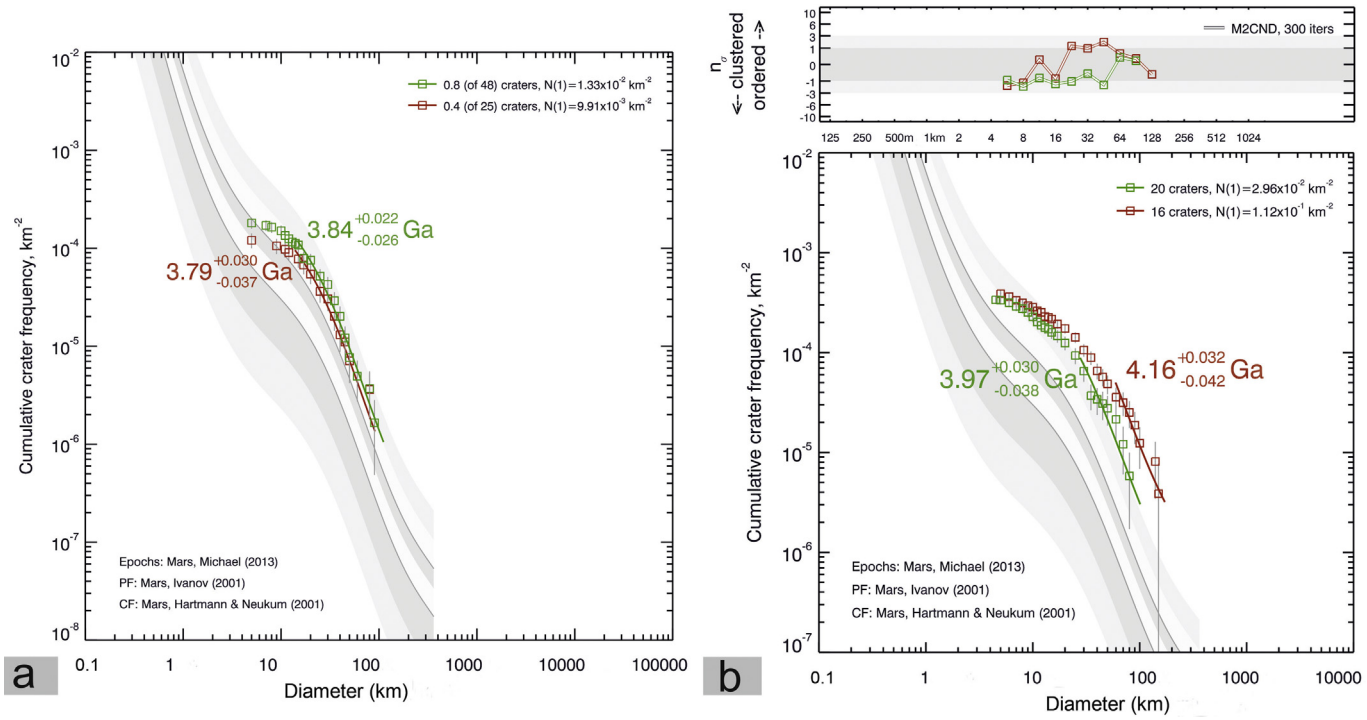


**Figure 3.** The CSFDs and derived model ages of area 1 (green), area 2 (red) (a) grabens. (b) Background ages of these grabens are shown following the same colour code. Fitting parameters are shown in Table 1.

early hundreds of million years (Schultz, 1985). Global contraction rates were of about 1.5–3 km (0.05%–0.1%) per billion years (Schubert et al., 1992), depending on crustal differentiation (Mangold et al., 2000). This contraction created elastic motion in the crust and thereafter accommodated this stress. Therefore, contraction resulted compressional tectonic features, when the stress reaches the maximal strength of the brittle crust (Mangold et al., 2000).

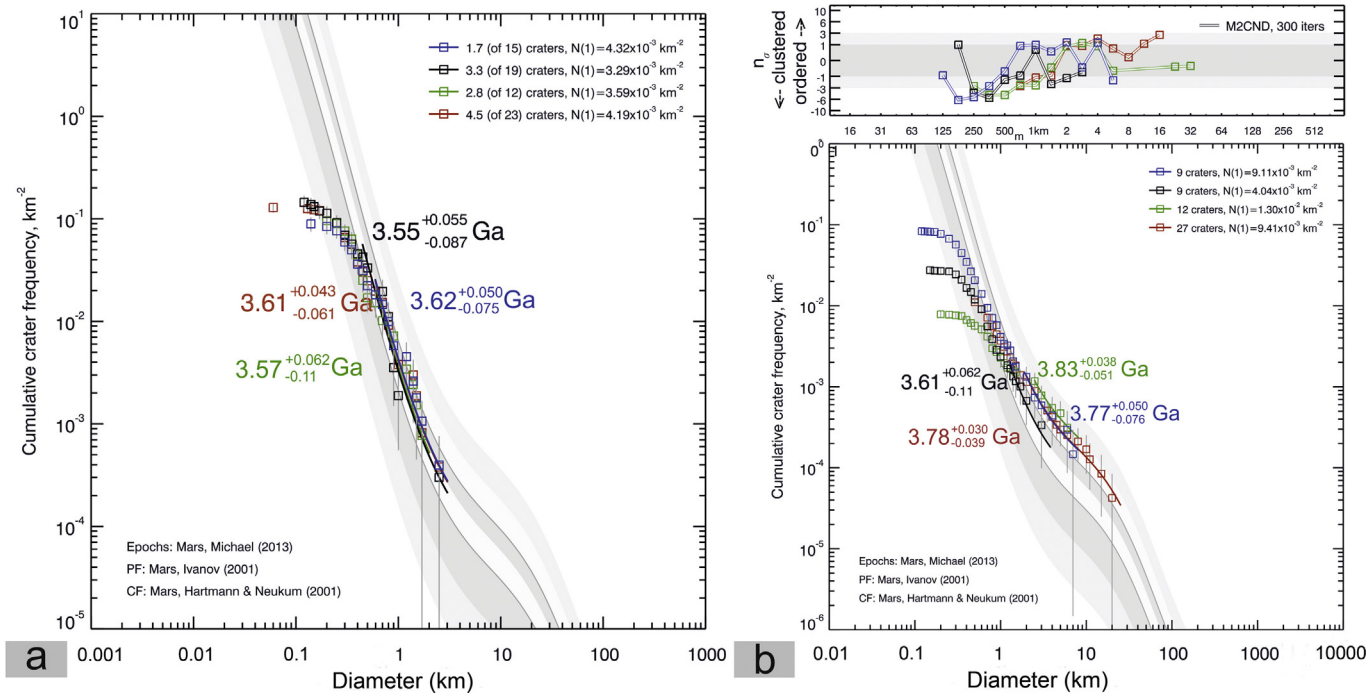


**Figure 4.** The CSFDs and derived model ages of wrinkle ridges in location 1 (blue), location 2 (black), location 3 (green), location 4 (red) (a) and background ages of locations 1, 2, 3, 4 in same color (b). Fitting parameters are shown in Table 1.

## 3. Methodology

Absolute age determination method of the planetary surface has been described by several scientists (Hartmann et al., 1981; Neukum, 1983; Hartmann and Neukum, 2001; Ivanov, 2001). The main hypothesis is based on the concept to fit the number of observed crater size frequency distribution (SFD) of a geologically symmetrical unit to a known crater production function (PF) (Michael and Neukum, 2010). Thereafter, the crater frequency for certain crater sizes coupled with chronology function (CF) is used to extract the absolute age (Michael and Neukum, 2010). Although, PF describes the number of craters of a given size are formed in relation to the number of any other size (Ivanov, 2001) and is determined by crater size-frequency distribution of a homogeneous surface on Mars and Moon (Michael and Neukum, 2010).

Studies to extract the age of tectonic structures were mostly conducted by determining the stratigraphic and crosscutting relations among the rock materials (i.e., geologic map units with relative ages based on stratigraphy and crater counts) and the tectonic structures. More specifically, the relative ages of the tectonic structures were based on stratigraphic and crosscutting relationships within the established stratigraphic system (Tanaka, 1986). Such relative-age assignments of extensional structures on the maps have adhered to the following guidelines (1) structures of younger age (e.g., Amazonian) may extend across boundaries of older units (e.g., Noachian and Hesperian), (2) structures of intermediate age (Hesperian) may extend into older units (e.g., Noachian) but not into younger units (Amazonian), and Noachian structures solely occur only in Noachian units. Clearly, this is a conservative approach and some structures that are wholly confined to their host units and not in contact with younger units, might be younger. Therefore, to better constrain the age uncertainty of tectonic structures in the mapping area, we attempt to determine ages directly using the BCC method.

The BCC technique was initially introduced by Tanaka (1982) by the name “Crater line count method” and performed by other investigators including Wichmann and Schultz (1989) with some modification. Fassett and Head (2008) introduced the term BCC in their publication. While BCC on Mars was mainly performed on the channel systems to determine their relative age of formation (Fassett and Head, 2008), Smith et al. (2009) and Kneissl et al. (2015) used it to determine the relative age of tectonic features on Mars.

BCC counts include all superposed impact craters that postdate the grabens (impacts that have modified both the structure and the materials deformed by the structure) with their centers located inside the bounding area of the mapped graben. The aim is to comprehensively include more impact craters to increase the statistical relevance of the analyzed data. The buffer depends on the diameter of the considered crater, i.e., the buffer applied for an impact crater with diameter larger than the buffer applied for a small diameter crater. To avoid the influence of later volcanism (Ody et al., 2013), which includes possible bimodal ages (i.e., both the age of the ancient crust and the age of the younger lavas), we have mapped and considered the craters that are solely in relation with the both bounding margins (i.e., opposite facing parallel normal faults) of the grabens. For the ages of the homogeneous surface, we mapped the craters that include their centers sharply inside the bounded area. In cases, we even made use of the superposed craters even if they are much larger than the actual width of the linear feature and thus their centers were outside the counting area (Tanaka, 1982; Kneissl et al., 2011). Craters were also included when the crater ejecta blanket superimposes the linear features (Kneissl et al., 2015). This helped to increase the number of craters for the statistical analysis as well as increased the buffer width.

CSFD of a similar-looking crust (similar albedo feature) helped to obtain the background ages of the graben, wrinkle ridge and lobate scarp-rich areas. Larger craters (>5.0 km for the grabens, >0.5 km for wrinkle ridges) were taken for consideration excluding small craters to avoid secondary craters. Special attention was paid to avoid crater chains to exclude the possibility of contaminating the data by counting potential secondary craters.

We identified a population of impact craters emplaced later than the formation of the linear structure in a certain accumulation area. This allowed us to find the population density required for the chronology model. Detailed observation revealed that there is a possibility that some craters could be syntectonic. A crater uplifted during the period of formation might appear very similar to one that was emplaced on top of the ridge structures later. Therefore, in some cases we restricted our investigation to portions of the ridges showing scarps or well-defined steep scarp-like boundaries. In such cases, we were able to identify whether a crater cuts the scarp. This indicates that the crater formed later or the scarp cuts the crater, and that the crater was pre-existing (Yue et al., 2017).

## 4. Data sets and software

Mapping was performed by examining imagery along with elevation data at different scales, from the Mars Orbiter Laser Altimeter (MOLA) (Smith et al., 1999) at ~463 m/pixel. Digital Elevation Models (DEM) extracted from high-resolution stereo camera (HRSC) images at ~12.5–50 m/pixel (Neukum and Jaumann, 2004; Jaumann et al., 2007) were also used wherever available. For the age determination, we mapped the tectonic structures (Supplementary files 1 and 2) using relatively high-resolution HRSC (12.5–25 m/pixel) and Context camera (CTX) (~6 m/pixel) images (Malin et al., 2007). THEMIS daytime images (Christensen et al., 2004) were also useful for primary identification of major structures. Map (Supplementary file 1) was shown on using ‘Lambert Conformal Conic Projection’ as mapped structures including volcanoes around Hellas basin reaches upto 70°S latitude. Thereafter, the structures were crater counted on an ArcGIS 10.2.2 platform. CraterTools (Kneissl et al., 2011), an ArcGIS add-on, eased to perform crater counting process and thereafter, counted craters were analyzed using CraterStats II (Michael, 2013). The newer version of the CraterTools is independent to projection system (Kneissl et al., 2011).

## 5. Results

Here in this study, we used the ‘simple buffer’ approach (buffer width = 1R) (where only superimposed craters were taken into consideration; Tanaka, 1982; Wichmann and Schultz, 1989; Senthil Kumar et al., 2016; van der Bogert et al., 2018) to calibrate the buffer width for the lobate scarps. The ‘Simple buffer’ approach was applied to small scale lobate scarps as it was difficult to discern crater ejecta crosscut the scarps due to the overall small sizes of the measured craters (Supplementary file 1; page 2). Therefore, to avoid uncertainties, we counted only the overprinting craters. However, grabens are very large-scale structures. At times, ejecta were visible even on the graben floors. We used the ‘ejecta’ approach (buffer width = 3R) for the grabens (Supplementary file 1; page 2). This is the same approach used by Fassett and Head (2008). Buffer width = 2R was used for the wrinkle ridges, where some rampart craters (with fluidized ejecta features) made it easy to understand the overprinting nature (Supplementary file 1; page 2). However, Kneissl et al. (2015) has clearly shown (Fig. 4D in their publication) there is not a

significant difference in derived age on the buffer width; it is only to increase statistical significance.

### 5.1. BCC analysis on grabens

Two definite non-Hellas concentric sets of grabens from 'areas 1 and 2' were selected for BCC analysis from the map (Supplementary file 1). The derived CSFD measurements for the area 1 grabens indicate a model age of 3.84 (+0.022/−0.026) Ga. Area 2 grabens have a derived AMA of 3.79 (+0.03/−0.037) Ga (Fig. 3a). From these acquired ages, we summarize that the extensional phase was dominant around 3.80 Ga (detail statistics on Table 1).

### 5.2. BCC analysis on wrinkle ridges and lobate scarps

Our map (Supplementary file 1) indicates the presence of a dominant alignment trend of shortening features due NNW–SSE in the highland region. Wrinkle ridges and lobate scarps are complex basement structural fabrics related to contraction, which originated due to compression (Watters, 1993; Mueller and Golombek, 2004). Therefore, their AMAs imply ages of latest operative compressional stress. The BCC derived ages of the wrinkle ridges in locations 1, 2, 3 and 4 are measured to be 3.62 (+0.050/−0.075) Ga, 3.55 (+0.055/−0.087) Ga, 3.57 (+0.062/−0.11) Ga and 3.61 (+0.043/0.061) Ga, respectively (detail statistics on Table 1) (Fig. 4). The ages of the lobate scarps from the rugged highland in locations 1 and 2 are 3.48 (+0.055/0.15) Ga and 3.55 (+0.065/−0.12) Ga (detail statistics on Table 1) (Fig. 5).

**Table 1**
Summary of AMAs of the linear/curvilinear structures and their background ages. Background ages (by CSFD) imply the age of the surface/basement where the linear structure formed.

| Unit | No. of fitted craters | Crater retention age N (1) | Absolute model age (Ga) | Error (Ga) | Fitted diameter range (km) |
|---|---|---|---|---|---|
| Graben Area 1 | 48 | $1.33 \times 10^{-2}$ | 3.84 | 0.022 −0.026 | 15–110 |
| Background | 20 | $2.96 \times 10^{-2}$ | 3.97 | 0.03 −0.038 | 28–100 |
| Graben Area 2 | 25 | $1.31 \times 10^{-2}$ | 3.79 | 0.03 −0.049 | 14–90 |
| Background | 16 | $1.12 \times 10^{-1}$ | 4.16 | 0.032 −0.042 | 60–170 |
| Wrinkle ridge Location 1 | 15 | $4.32 \times 10^{-3}$ | 3.62 | 0.05 −0.075 | 0.6–3 |
| Background | 9 | $9.11 \times 10^{-3}$ | 3.77 | 0.05 −0.076 | 1.9–8 |
| Wrinkle ridge Location 2 | 19 | $3.29 \times 10^{-3}$ | 3.55 | 0.055 −0.087 | 0.45–3 |
| Background | 9 | $4.04 \times 10^{-3}$ | 3.61 | 0.062 −0.11 | 1.3–3.8 |
| Wrinkle ridge Location 3 | 12 | $3.59 \times 10^{-3}$ | 3.57 | 0.062 −0.11 | 0.6–2 |
| Background | 12 | $1.3 \times 10^{-2}$ | 3.83 | 0.038 −0.051 | 2.5–8 |
| Wrinkle ridge Location 4 | 23 | $4.19 \times 10^{-3}$ | 3.61 | 0.043 −0.061 | 0.6–3 |
| Background | 27 | $9.41 \times 10^{-3}$ | 3.78 | 0.03 −0.039 | 2–25 |
| Lobate scarp Location 1 | 14 | $2.68 \times 10^{-3}$ | 3.48 | 0.075 −0.15 | 0.425–1.5 |
| Background | 5 | $4.05 \times 10^{-2}$ | 4.01 | 0.055 −0.09 | 3.5–20 |
| Lobate scarp Location 2 | 12 | $3.55 \times 10^{-3}$ | 3.55 | 0.065 −0.12 | 0.43–0.86 |
| Background | 16 | $2.25 \times 10^{-2}$ | 3.92 | 0.034 −0.045 | 2.5–30 |

### 5.3. Tectonic structures in the southern highlands and their relation to internal processes

The trends and morphologies of grabens within areas 1 and 2 differ (Ruj et al., 2017; Supplement file 2) differ from typical basin-concentric grabens found on lunar, Martian and Ganymede's crusts, which were formed by impact-related stresses and later 'Mascon' adjustment of the impact basin (Melosh et al., 2013). Major lunar mare basins have a well-documented history of repeated vertical movement and subsidence related tectonic features in response to super isostatic loading by mare basalt fill (Melosh et al., 2013). According to Wichmann and Schultz (1989), concentric "canyons" form outside the basin boundary scarp at or near the time of basin formation (here the grabens of area 1 and 2 are approximately 150–200 Ma younger). These types of grabens reach maximum widths of 20 km on Mars (Golombek and McGill, 1983; Tanaka et al., 2014) and are adjacent to the rim of the basin (Golombek and McGill, 1983; Tanaka et al., 2014). After a hiatus, concentric grabens develop inside the basin within the massif ring. However, in this case, due to the giant size of the Hellas basin interior melt pool, the conductive cooling time probably exceeds millions of years (Elkins-Tanton et al., 2011) to attain visco-elastic relaxation. In contrast, area 1 and 2 grabens are much wider, 100 km and 30 km wide respectively, and approximately 1200 km away from the basin's outer rim. The investigated area 1 and 2 grabens have distinct orientations (antithetic to outer arc curvature) and morphologies (not centered around the giant Hellas impact basins, either concentrically or radially), but they have similar ages.

While investigating the eastern part of the Hellas basin (Supplementary file 1), we observed approximately 800 km long and relatively straight trails of Dao and Harmakhis Valles (Glamoclija et al., 2011, and references therein) have a similar trend to the area 1 grabens. This might be due to structural control of the channels (where channels tend to follow the week zones created by the pre-existing suture zone), which is commonly observed on Earth, particularly in the Rhine river valley (Preusser, 2008, and references therein) and the Narmada river valley in India (Biswas, 1987, and references therein). Similar examples of basement structural control on the formation of Martian valley networks are observed in the Thaumasia region (Dohm and Tanaka, 1999), where valleys follow a certain week zone. We do not exclude the possibility that these channels are slope controlled (Crown et al., 1992), even though their noted lengths and overall similarity in trend to area 1 grabens over such long length is intriguing.

With an extensive area of >2.1 million km$^2$, the six oldest central vents of volcanoes in the Martian highlands (Supplementary file 1) formed after the Hellas impact basin, between 4.0 Ga and 3.7 Ga (Williams et al., 2009). The alignment of volcanic chains (namely the circum-Hellas volcanic province by Crown et al., 1992; Williams et al., 2009) in Hellas and the surrounding regions, including northeastern Tyrrhenus Mons, Hadriacus Mons, southern Peneus Patera, Amphitrites Patera, Malea Patera and Pityusa Patera, follow a general linearity (Fig. 2 in Leone, 2016). Tectonics and association of volcanism are well studied on both Earth (Ferguson et al., 2010) and Mars (Carr, 1973; Harder and Christensen, 1996; Zhong, 2009) as volcanoes tend to follow weak zones created by faults (Leone, 2016) or sometimes vice-versa. We also suspect that circum-Hellas volcanics might be related to area 1 grabens with similar formational mechanism. This possibility rises due to the similarity in the trend of the grabens and the alignment of the similar aged circum-Hellas volcanics (Williams et al., 2009).

In absence of typical Earth-like plate tectonic scenario the possible origin of the stress related to the origin of the extensional structures could be lithospheric stretching. Lithospheric stretching is a common phenomenon on Earth and Mars (Sleep, 1994;

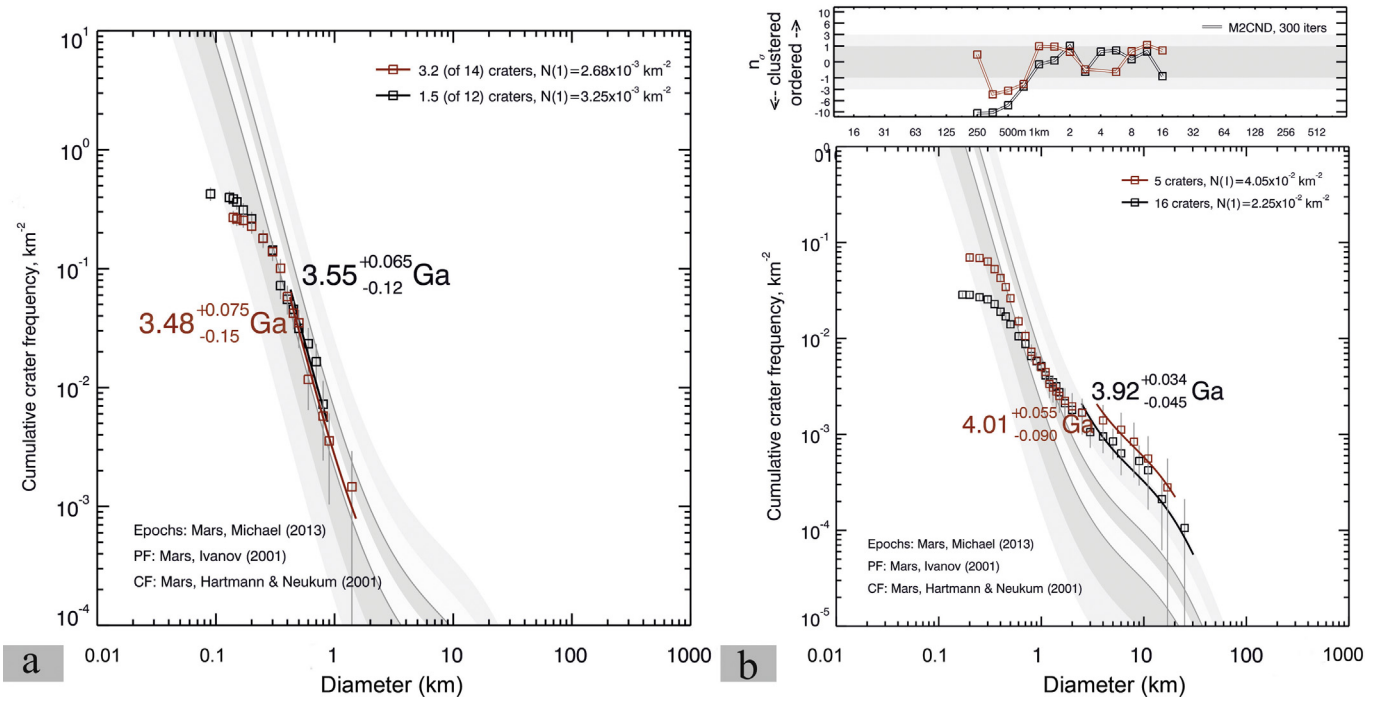


**Figure 5.** The CSFDs and derived model ages of lobate scarp of location 1 (black), location 2 (red) (a) and background ages of locations 1 and 2 in same color (b). Fitting parameters are shown in Table 1.

Anderson et al., 2008), which might lead to extension and formation of grabens in the western part of the Hellas basin. This imposed stress field resulted due to vertical shortening that may have been triggered by gravitational collapse of the Hellas basin during the later phase of isostatic basin adjustment (Sjorgren and Wimberley, 1981). It is concluded from the derived AMAs that the lithospheric activity (around 3.8 Ga) did not shut down after the Hellas and Argyre impact events (3.99 Ga for Hellas, 3.93 Ga for Argyre) but lithospheric mobility continued after those impact events.

Another possible formation mechanism of the investigated extensional structures could be related to the possibility of the presence of an underlying plume (Leone, 2016), similar to the Tharsis at the similar time (Mège and Masson, 1996), pushing the lithosphere from below. The diapir created by an uprising plume impinges on the base of lithosphere. It spreads out radially, eventually resulting in the uplift of the crust (or as circular plateau) and creating extensional fractures depending on the thickness of the upper lithosphere and the size of the diapir.

On the contrary, the stress mechanism related to formation of compressional structures is simpler and well established (Mangold et al., 2000; Andrews-Hanna et al., 2008). Watters (1993) believed that slow cooling of the planet interior and monotonic decrease in volcanism and lithospheric strain rates were responsible for their formation. An Early Hesperian pulse of global volcanism, related to the thermal evolution of the planet might have resulted in a punctuated episode of rapid cooling and thereafter, global contraction that contributed to global compressional tectonism during that period (Mangold et al., 2000). Compression structures (especially wrinkle ridges) are more dominant in the northern part of the investigated region (mainly Terra Sabaea). Late Noachian volcanism (Carr, 1973) is corroborated by the estimated background ages (lava floored material) of the wrinkle ridges (Table 1). These ages also are also consistent with the ages of the grabens (i.e., around 3.8 Ga), derived in this study and the ages of volcanics of Syrtis Major and Hesperia Planum (Carr, 1973). All these correspond to the stress field for the grabens and the volcanism in the eastern Hellas region (circum-Hellas volcanic province).

The estimated age of the grabens, of approximately 3.80 Ga, depicts the latest extensional activity associated with graben formation in central Noachis Terra (also possibly later reactivation of a pre-existing tectonic structure). The general trend of the grabens, especially area 1, is probably influenced by pre-existing weak zones created by NNE–SSW trending transform faults (mentioned as "great fault") system interpreted through magnetic data (Connerney et al., 2005). This magnetic anomaly was an event prior to the giant impacts such as Hellas. Fig. 6 summarizes the history of the evolution of this mapped region.

The thermal history models for Mars (Schubert and Spohn, 1990; Schubert et al., 1992) are quantitatively consistent with the derived timings of the operated stresses in this study. Schubert and Spohn (1990) suggested that an extended period of planetary expansion, extensional tectonics and widespread volcanism involved in cooling initial temperatures over the bulk of the planet and a later global differentiation relative to the other terrestrial planets. This model also predicts subsequent planetary cooling and related contraction inducing global compressive horizontal stress in the lithosphere sufficient (>1 kbar) to produce compressional tectonic features on the Martian surface (Solomon, 1978).

## 6. Summary and conclusions

Our investigations from surface structural expressions indicate that the Noachis-Sabaea region records a dynamic lithospheric activity. The BCC derived AMAs imply two distinct dominant phases of stress activities. An extensional phase terminating at around 3.8 Ga and a compressional phase around 3.5–3.6 Ga. Extensional features prior to 3.8 Ga have been frequently observed on Mars, but prevail entirely as a western hemispheric (Golombek and Phillips, 2010) phenomenon, related to the incipient development of Tharsis and its components (Anderson et al., 2001).

In this study the AMAs of the grabens are indicated to be the same irrespective of orientations and locations, implying the presence of a similar regional crustal structure over an extensive part of southern

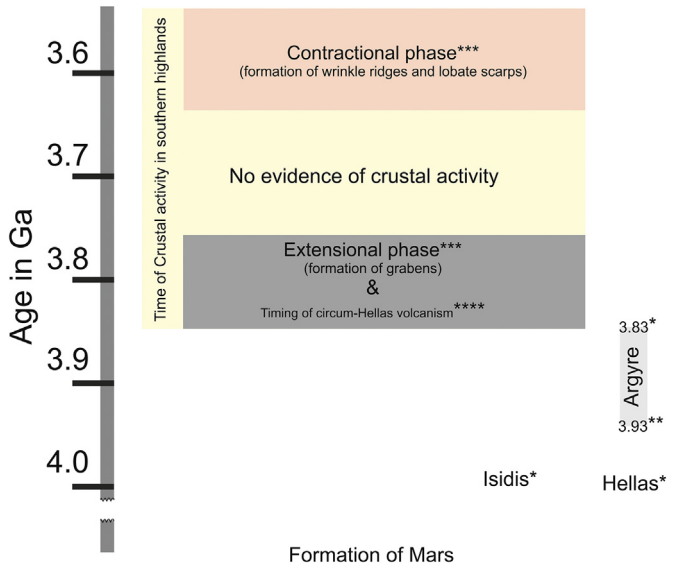


**Figure 6.** Tectonic evolution of the study area in relation to the giant impact events forming the Agyre, Isidis, and Hellas basins. Ages derived by * Werner (2008), ** Robbins et al. (2013), *** Derived in this study, **** Williams et al. (2009).

highlands. As clear plate boundaries are not identified at least on the presently exposed Martian surface, the plate tectonic theory does not have strong support and it remains a hypothesis. Nonetheless, the justification behind the origin of the horizontal stresses related to the formation of these grabens indicates lithospheric stretching around 3.8 Ga. In this case, the weight of the overlying material and the Hellas basin's isostatic adjustment (Sjorgren and Wimberley, 1981; Melosh et al., 2013) caused lateral spreading most likely due to gravitational collapse. Gravitationally unstable dynamic topography triggered gravitational collapse leading to the formation of the extensional structures (Emishaw et al., 2017).

Wrinkle ridges and lobate scarps approximately around 3.5–3.6 Ga correspond to the peak of the global contractional phase related to the planetary cooling (Andrews-Hanna et al., 2008). Scott and Dohm (1990) argued variable effects of uplift, flexural loading and isostatic adjustment resulting from the evolution of Tharsis. Our derived ages match with the Martian thermal history model proposed by Schubert and Spohn (1990). They argued that after a short period of extension following planet accretion, a relatively high compressional strain rate existed in the lithosphere for billions of years and was succeeded by a progressively lower compressional strain as the interior temperature dropped. Consistent and similar orientations of the wrinkle ridges and lobate scarps reflect that stresses spread evenly over an enormous distance on a single-plate (Plescia and Golombek, 1986) planet, at least during a later stage of Mars' crustal evolution. Therefore, the extensional structures were dominant (at around 3.8 Ga) on a particular area with multiple orientations (Anderson et al., 2001, 2008) whereas compressional activity (around 3.5–3.6 Ga) had an impact all over the planet at a similar period (Watters, 1993). This model differs from Earth where deformations are concentrated over relatively small regions due to mobile plate boundaries.

## Acknowledgements

JMD was partially supported by JSPS KAKENHI (Grant-in-Aid for Scientific Research on Innovative Areas) Grant No. 26106002 (Hadean Bio-Science). TR acknowledges Prof. Harald Hiesinger for providing his laboratory facilities during the crater counting phase. Discussions with him and Prof. Misha Ivanov during the early phase of manuscript preparation were extremely beneficial. TR also thanks Gene W. Schmidt for going through the English grammar of the manuscript and putting valuable comments to improve it. We are grateful to the two anonymous reviewers for their comments to improve the quality of the manuscript.

## Appendix A. Supplementary data

Supplementary data related to this article can be found at https://doi.org/10.1016/j.gsf.2018.05.016.

## References

Anderson, R.C., Dohm, J.M., Golombek, M.P., Haldemann, A., Franklin, B.J., Tanaka, K.L., Lias, J., Peer, B., 2001. Primary centers and secondary concentrations of tectonic activity through time in the western hemisphere of Mars. Journal of Geophysical Research Planets 106, 20,563–20,586. https://doi.org/10.1029/2000JE001278.

Anderson, R.C., Dohm, J.M., Haldemann, A.F.C., Pounders, E., Golombek, M., Castano, A., 2008. Centers of tectonic activity in the eastern hemisphere of Mars. Icarus 195 (2), 537–546. https://doi.org/10.1016/j.icarus.2007.12.027.

Andrews-Hanna, J.C., Zuber, M.T., Hauck, S.A., 2008. Strike-slip faults on Mars: observations and implications for global tectonics and geodynamics. Journal of Geophysical Research Planets 113 (E8). https://doi.org/10.1029/2007JE002980.

Baker, V.R., Maruyama, S., Dohm, J.M., 2002. A theory of early plate tectonics and subsequent long-term superplume activity on Mars. In: International Workshop: Role of Superplumes in the Earth System, Electronic Geosciences, vol. 7, pp. 312–316.

Baker, V.R., Maruyama, S., Dohm, J.M., 2007. Tharsis superplume and the geological evolution of early Mars. In: Superplumes: Beyond Plate Tectonics. Springer, Netherlands, pp. 507–522. https://doi.org/10.1007/978-1-4020-5750-2_17.

Biswas, S.K., 1987. Regional tectonic framework, structure and evolution of the western marginal basins of India. Tectonophysics 135 (4), 307–327. https://doi.org/10.1016/0040-1951(87)90115-6.

Carr, M.H., 1973. Volcanism on Mars. Journal of Geophysical Research 78 (20), 4049–4062. https://doi.org/10.1029/JB078i020p04049.

Chicarro, A.F., Schultz, P.H., Masson, P., 1985. Global and regional ridge patterns on Mars. Icarus 63 (1), 153–174. https://doi.org/10.1016/0019-1035(85)90025-9.

Christensen, P.R., Jakosky, B.M., Kieffer, H.H., Malin, M.C., McSween, H.Y., Nealson, K., Mehall, G.L., Silverman, S.H., Ferry, S., Caplinger, M., Ravine, M., 2004. The thermal emission imaging system (THEMIS) for the Mars 2001 Odyssey Mission. Space Science Reviews 110 (1–2), 85–130.

Connerney, J.E.P., Acuña, M.H., Ness, N.F., Kletetschka, G., Mitchell, D.L., Lin, R.P., Reme, H., 2005. Tectonic implications of Mars crustal magnetism. Proceedings of the National Academy of Sciences of the United States of America 102 (42), 14970–14975. https://doi.org/10.1073/pnas.0507469102.

Crown, D.A., Price, K.H., Greeley, R., 1992. Geologic evolution of the east rim of the Hellas basin, Mars. Icarus 100, 1–25. https://doi.org/10.1016/0019-1035(92)90014-X.

Dohm, J.M., 2017. Summarized evolution of Mars. In: Lunar and Planetary Science Conference (Vol. 48), 2007, March.

Dohm, J.M., Maruyama, S., 2014. Habitable trinity. Geoscience Frontiers 6, 95–101. https://doi.org/10.1016/j.gsf.2014.01.005.

Dohm, J.M., Tanaka, K.L., 1999. Geology of the Thaumasia region, Mars: plateau development, valley, and magmatic evolution. Planetary and Space Science 47, 411–431. https://doi.org/10.1016/S0032-0633(98)00141-X.

Elkins-Tanton, L.T., Burgess, S., Yin, Q.Z., 2011. The lunar magma ocean: reconciling the solidification process with lunar petrology and geochronology. Earth and Planetary Science Letters 304 (3–4), 326–336. https://doi.org/10.1016/j.epsl.2011.02.004.

Emishaw, L., Laó-Dávila, D.A., Abdelsalam, M.G., Atekwana, E.A., Gao, S.S., 2017. Evolution of the broadly rifted zone in southern Ethiopia through gravitational collapse and extension of dynamic topography. Tectonophysics 699, 213–226. https://doi.org/10.1016/j.tecto.2016.12.009.

Fassett, C.I., Head III, J.W., 2008. The timing of Martian valley network activity: constraints from buffered crater counting. Icarus 195 (1), 61–89. https://doi.org/10.1016/j.icarus.2007.12.009.

Ferguson, D.J., Barnie, T.D., Pyle, D.M., Oppenheimer, C., Yirgu, G., Lewi, E., Kidane, T., Carn, S., Hamling, I., 2010. Recent rift-related volcanism in Afar, Ethiopia. Earth and Planetary Science Letters 292 (3), 409–418. https://doi.org/10.1016/j.epsl.2010.02.010.

Glamoclija, M., Marinangeli, L., Komatsu, G., 2011. Harmakhis Vallis Source Region, Mars: insights into the recent geothermal history based on geological mapping. Planetary and Space Science 59, 1179–1194. https://doi.org/10.1016/j.pss.2010.09.017.

Golombek, M.P., McGill, G.E., 1983. Grabens, basin tectonics, and the maximum total expansion of the Moon. Journal of Geophysical Research Solid Earth 88 (B4), 3563–3578. https://doi.org/10.1029/JB088iB04p03563.

Golombek, M.P., Phillips, R.J., 2010. Mars tectonics. Planetary Tectonics 11, 183–232.

Harder, H., Christensen, U.R., 1996. A one-plume model of Martian mantle convection. Nature 380 (6574), 507. https://doi.org/10.1038/380507a0.

Hartmann, W.K., Strom, R.G., Weidenschilling, S.J., Blasius, K.R., Voronow, A., Dence, M.R., Grieve, R.A.F., Diaz, J., Chapman, C.R., Shoemaker, E.M., Jones, K.L., 1981. Basaltic Volcanism on the Terrestrial Planets. Pergamon Press, New York, 2, p.3.
Hartmann, W.K., Neukum, G., 2001. Cratering chronology and the evolution of Mars. Space Science Reviews 96 (1), 165–194. https://doi.org/10.1023/A:1011945222010.
Hiesinger, H., Head, J.W., 2004. The Syrtis Major volcanic province, Mars: synthesis from Mars global surveyor data. Journal of Geophysical Research Planets 109 (E1). https://doi.org/10.1029/2003JE002143.
Hopkins, M.D., Mojzsis, S.J., 2015. A protracted timeline for lunar bombardment from mineral chemistry, Ti thermometry and U–Pb geochronology of Apollo 14 melt breccia zircons. Contributions to Mineralogy and Petrology 169 (3), 30. https://doi.org/10.1007/s00410-015-1123-x.
Ivanov, B.A., 2001. Mars/Moon cratering rate ratio estimates. Space Science Reviews 96 (1), 87–104. https://doi.org/10.1023/A:1011941121102.
Ivanov, B.A., Neukum, G., Wagner, R., 2001. Size-frequency distributions of planetary impact craters and asteroids. In: Collisional Processes in the Solar System, vol. 261. Springer, Dordrecht, pp. 1–34.
Jaumann, R., Neukum, G., Behnke, T., Duxbury, T.C., Eichentopf, K., Flohrer, J., Gasselt, S.V., Giese, B., Gwinner, K., Hauber, E., Hoffmann, H., 2007. The high-resolution stereo camera (HRSC) experiment on Mars Express: instrument aspects and experiment conduct from interplanetary cruise through the nominal mission. Planetary and Space Science 55 (7–8), 928–952. https://doi.org/10.1016/j.pss.2006.12.003.
Kneissl, T., van Gasselt, S., Neukum, G., 2011. Map-projection-independent crater size-frequency determination in GIS environments—new software tool for ArcGIS. Planetary and Space Science 59 (11), 1243–1254. https://doi.org/10.1016/j.pss.2010.03.015.
Kneissl, T., Michael, G.G., Platz, T., Walter, S.H.G., 2015. Age determination of linear surface features using the Buffered Crater Counting approach–Case studies of the Sirenum and Fortuna Fossae graben systems on Mars. Icarus 250, 384–394. https://doi.org/10.1016/j.icarus.2014.12.008.
Leone, G., 2016. Alignments of volcanic features in the southern hemisphere of Mars produced by migrating mantle plumes. Journal of Volcanology and Geothermal Research 309, 78–95. https://doi.org/10.1016/j.jvolgeores.2015.10.028.
Malin, M.C., Bell, J.F., Cantor, B.A., Caplinger, M.A., Calvin, W.M., Clancy, R.T., Edgett, K.S., Edwards, L., Haberle, R.M., James, P.B., Lee, S.W., 2007. Context camera investigation on board the Mars reconnaissance orbiter. Journal of Geophysical Research Planets 112 (E5). https://doi.org/10.1029/2006JE002808.
Mangold, N., Allemand, P., Thomas, P.G., 1998. Wrinkle ridges of Mars: structural analysis and evidence for shallow deformation controlled by ice-rich décollements. Planetary and Space Science 46 (4), 345–356. https://doi.org/10.1016/S0032-0633(97)00195-5.
Mangold, N., Allemand, P., Thomas, P.G., Vidal, G., 2000. Chronology of compressional deformation on Mars: evidence for a single and global origin. Planetary and Space Science 48 (12–14), 1201–1211. https://doi.org/10.1016/S0032-0633(00)00104-5.
Maruyama, S., Ebisuzaki, T., 2017. Origin of the Earth: a proposal of new model called ABEL. Geoscience Frontiers 8 (2), 253–274. https://doi.org/10.1016/j.gsf.2016.10.005.
Mège, D., Masson, P., 1996. Stress models for Tharsis formation, Mars. Planetary and Space Science 44 (12), 1471–1497. https://doi.org/10.1016/S0032-0633(96)00112-2.
Melosh, H.J., Freed, A.M., Johnson, B.C., Blair, D.M., Andrews-Hanna, J.C., Neumann, G.A., Phillips, R.J., Smith, D.E., Solomon, S.C., Wieczorek, M.A., Zuber, M.T., 2013. The origin of lunar mascon basins. Science 340 (6140), 1552–1555. https://doi.org/10.1126/science.1235768.
Michael, G.G., Neukum, G., 2010. Planetary surface dating from crater size–frequency distribution measurements: partial resurfacing events and statistical age uncertainty. Earth and Planetary Science Letters 294 (3–4), 223–229. https://doi.org/10.1016/j.epsl.2009.12.041.
Michael, G.G., 2013. Planetary surface dating from crater size–frequency distribution measurements: multiple resurfacing episodes and differential isochron fitting. Icarus 226 (1), 885–890. https://doi.org/10.1016/j.icarus.2016.05.019.
Mueller, K., Golombek, M., 2004. Compressional structures on Mars. Annual Reviews of Earth Planetary Science 32, 435–464. https://doi.org/10.1146/annurev.earth.32.101802.120553.
Nahm, A.L., Schultz, R.A., 2011. Magnitude of global contraction on Mars from analysis of surface faults: implications for Martian thermal history. Icarus 211 (1), 389–400. https://doi.org/10.1016/j.icarus.2010.11.003.
Neukum, G., 1983. Meteoritenbombardement und datierung planetarer oberflachen. Habilitation Dissertation for Faculty Membership. Ludwig Maximilianis Univ.
Neukum, G., Jaumann, R., 2004. August. HRSC: the high resolution stereo camera of Mars Express. In: Mars Express: The Scientific Payload (V. 1240, 17-35), pp. 17–35. ISBN 92-9092-556-6.
Ody, A., Poulet, F., Bibring, J.P., Loizeau, D., Carter, J., Gondet, B., Langevin, Y., 2013. Global investigation of olivine on Mars: insights into crust and mantle compositions. Journal of Geophysical Research Planets 118 (2), 234–262. https://doi.org/10.1029/2012JE004149.
Plescia, J.B., Golombek, M.P., 1986. Origin of planetary wrinkle ridges based on the study of terrestrial analogs. Geological Society of America Bulletin 97 (11), 1289–1299. https://doi.org/10.1130/0016-7606(1986)97.
Preusser, F., 2008. Characterisation and evolution of the river rhine system. Netherlands Journal of Geosciences 87 (01), 7–19. https://doi.org/10.1017/S0016774600024008.
Robbins, S.J., Hynek, B.M., Lillis, R.J., Bottke, W.F., 2013. Large impact crater histories of Mars: the effect of different model crater age techniques. Icarus 225 (1), 173–184. https://doi.org/10.1016/j.icarus.2013.03.019.
Rogers, A.D., Nazarian, A.H., 2013. Evidence for Noachian flood volcanism in Noachis Terra, Mars, and the possible role of Hellas impact basin tectonics. Journal of Geophysical Research Planets 118 (5), 1094–1113. https://doi.org/10.1002/jgre.20083.
Ruj, T., Komatsu, G., Dohm, J.M., Miyamoto, H., Salese, F., 2017. Generic identification and classification of morphostructures in the Noachis-Sabaea region, southern highlands of Mars. Journal of Maps 13 (2), 755–766. https://doi.org/10.1080/17445647.2017.1379913.
Ruj, T., Komatsu, G., Pondrelli, M., Pietro, I.D., Pozzobon, R., 2018. Morphometric analysis of a Hesperian aged Martian lobate scarp using high-resolution data. Journal of Structural Geology 113, 1–9. https://doi.org/10.1016/j.jsg.2018.04.018.
Schubert, G., Spohn, T., 1990. Thermal history of Mars and the sulfur content of its core. Journal of Geophysical Research Solid Earth 95 (B9), 14095–14104. https://doi.org/10.1029/JB095iB09p14095.
Schubert, G., Soloman, S.C., Turcotte, D.L., Drake, M.J., Sleep, N.H., 1992. Origin and thermal evolution of Mars. In: Snyder, C.W., Kieffer, H.H., Jakosky, B.M., Matthew, M.S. (Eds.), Mars. The University of Arizona Press, Tuscon, pp. 147–183.
Schultz, R.A., 1985. Assessment of global and regional tectonic models for faulting in the ancient terrains of Mars. Journal of Geophysical Research Solid Earth 90 (B9), 7849–7860. https://doi.org/10.1029/JB090iB09p07849.
Scott, D.H., Dohm, J.M., 1990. Chronology and global distribution of fault and ridge systems on Mars. In: Lunar and Planetary Science Conference Proceedings (V. 20, 487–501).
Senthil Kumar, P., Sruthi, U., Krishna, N., Lakshmi, K.J.P., Menon, R., Gopala Krishna, B., Kring, D.A., Head, J.W., Goswami, J.N., Kiran Kumar, A.S., 2016. Recent shallow moonquake and impact-triggered boulder falls on the Moon: new insights from the Schrödinger basin. Journal of Geophysical Research Planets 121 (2), 147–179. https://doi.org/10.1002/2015JE004850.
Sjorgren, W.L., Wimberley, R.N., 1981. Mars: Hellas Planitia gravity analysis. Icarus 45 (2), 331–338. https://doi.org/10.1016/0019-1035(81)90038-5.
Sleep, N.H., 1994. Martian plate tectonics. Journal of Geophysical Research Planets 99 (E3), 5639–5655. https://doi.org/10.1029/94JE00216.
Smith, M.R., Gillespie, A.R., Montgomery, D.R., Batbaatar, J., 2009. Crater–fault interactions: a metric for dating fault zones on planetary surfaces. Earth and Planetary Science Letters 284 (1–2), 151–156. https://doi.org/10.1016/j.epsl.2009.04.025.
Smith, D.E., Zuber, M.T., Solomon, S.C., Phillips, R.J., Head, J.W., Garvin, J.B., Banerdt, W.B., Muhleman, D.O., Pettengill, G.H., Neumann, G.A., Lemoine, F.G., 1999. The global topography of Mars and implications for surface evolution. Science 284 (5419), 1495–1503. https://doi.org/10.1126/science.284.5419.1495.
Solomon, S.C., 1978. On volcanism and thermal tectonics on one-plate planets. Geophysical Research Letters 5 (6), 461–464. https://doi.org/10.1029/GL005i006p00461.
Tanaka, K.L., 1982. A New Time-saving Crater-count Technique, with Application to Narrow Features. NASA Technical Memo, NASA TM-85127, pp. 123–125.
Tanaka, K.L., 1986. The stratigraphy of Mars. Journal of Geophysical Research Solid Earth 91 (B13).
Tanaka, K.L., Robbins, S.J., Fortezzo, C.M., Skinner, J.A., Hare, T.M., 2014. The digital global geologic map of Mars: chronostratigraphic ages, topographic and crater morphologic characteristics and updated resurfacing history. Planetary and Space Science 95, 11–24. https://doi.org/10.1016/j.pss.2013.03.006.
van der Bogert, C.H., Clark, J.D., Hiesinger, H., Banks, M.E., Watters, T.R., Robinson, M.S., 2018. How old are lunar lobate scarps? 1. Seismic resetting of crater size-frequency distributions. Icarus 306, 225–242. https://doi.org/10.1016/j.icarus.2018.01.019.
Watters, T.R., 1993. Compressional tectonism on Mars. Journal of Geophysical Research Planets 98 (E9), 17049–17060. https://doi.org/10.1029/93JE01138.
Werner, S.C., 2008. The early Martian evolution—constraints from basin formation ages. Icarus 195 (1), 45–60. https://doi.org/10.1016/j.icarus.2007.12.008.
Wichmann, R.W., Schultz, P.H., 1989. Sequence and mechanisms of deformation around the Hellas and Isidis impact basins on Mars. Journal of Geophysical Research 94 (B12). https://doi.org/10.1029/JB094iB12p17333, 17–333.
Williams, D.A., Greeley, R., Fergason, R.L., Kuzmin, R., McCord, T.B., Combe, J.P., Head, J.W., Xiao, L., Manfredi, L., Poulet, F., Pinet, P., 2009. The circum-Hellas volcanic province, Mars: overview. Planetary and Space Science 57 (8), 895–916. https://doi.org/10.1016/j.pss.2008.08.010.
Yin, A., 2012. An episodic slab-rollback model for the origin of the Tharsis rise on Mars: implications for initiation of local plate subduction and final unification of a kinematically linked global plate-tectonic network on Earth. Lithosphere 4 (6), 553–593. https://doi.org/10.1130/L195.1.
Yue, Z., Michael, G.G., Di, K., Liu, J., 2017. Global survey of lunar wrinkle ridge formation times. Earth and Planetary Science Letters 477, 14–20. https://doi.org/10.1016/j.epsl.2017.07.048.
Zhong, S., 2009. Migration of Tharsis volcanism on Mars caused by differential rotation of the lithosphere. Nature Geoscience 2 (1), 19. https://doi.org/10.1038/ngeo392.
Zuber, M.T., Solomon, S.C., Phillips, R.J., Smith, D.E., Tyler, G.L., Aharonson, O., Balmino, G., Banerdt, W.B., Head, J.W., Johnson, C.L., Lemoine, F.G., 2000. Internal structure and early thermal evolution of Mars from Mars Global Surveyor topography and gravity. Science 287 (5459), 1788–1793. https://doi.org/10.1126/science.287.5459.1788.